

Supplementary Information

High Temperature Hydrothermal Synthesis of Rare-Earth Titanates: Synthesis and Structure of $RE_5Ti_4O_{15}(OH)$ ($RE = La, Er$), $Sm_3TiO_5(OH)_3$, $RE_5Ti_2O_{11}(OH)$ ($RE = Tm-Lu$) and $Ce_2Ti_4O_{11}$

Kyle Fulle, Liurukara. D. Sanjeeva, Colin D. McMillen, Joseph W. Kolis*

Department of Chemistry and Center for Optical Materials Science and Engineering Technologies (COMSET), Clemson University, Clemson, South Carolina 29634-0973, USA

Synthesis

- Synthesis of $La_5Ti_4O_{15}OH$ and $Er_5Ti_4O_{15}(OH)$
- Synthesis of $Lu_5Ti_2O_{11}(OH)$, $Yb_5Ti_2O_{11}(OH)$ and $Tm_5Ti_2O_{11}(OH)$
- Synthesis of $Sm_3TiO_5(OH)$
- Synthesis of $Ce_2Ti_4O_{11}$
- Synthesis of $RE_2Ti_2O_7$ ($RE = La, Pr, Nd, Gd-Lu$) Single Crystals

Structure Refinement of $Lu_5Ti_2O_{11}(OH)$

Table SI 1: Crystallographic data for hydrothermally grown $Er_5Ti_4O_{15}(OH)$.

Table SI 2: Selected bond lengths (Å) of $La_5Ti_4O_{15}(OH)$ and $Er_5Ti_4O_{15}(OH)$.

Table SI 3: Selected bond lengths (Å) of $Sm_3TiO_5(OH)_3$, $Lu_5Ti_2O_{11}(OH)$, and $Ce_2Ti_4O_{11}$.

Table SI 4: Bond valence sum calculations of $La_5Ti_4O_{15}(OH)$ and $Er_5Ti_4O_{15}(OH)$.

Table SI 5: Bond valence sum calculations of $Sm_3TiO_5(OH)_3$, $Lu_5Ti_2O_{11}(OH)$ and $Ce_2Ti_4O_{11}$.

Table SI 6: EDX of reported rare-earth titanates with experimental and expected RE:Ti ratios.

Table SI 7: Summary of $M-M$ bond distances for $RE_5M_2O_{12}$ ($M = Ru, Re$) and $RE_5Ti_2O_{11}(OH)$ compounds.

Figure SI 1: PXRD patterns of $La_5Ti_4O_{15}(OH)$. (a) Simulated powder pattern based on single crystal data of $La_5Ti_4O_{15}(OH)$; (b) Observed PXRD of $La_5Ti_4O_{15}(OH)$.

Figure SI 2: PXRD patterns of $Sm_3TiO_5(OH)_3$. (a) Simulated powder pattern based on single crystal structure data of $Sm_3TiO_5(OH)_3$; (b) Observed PXRD pattern for the $Sm_3TiO_5(OH)_3$ reaction and impurities of $Sm(OH)_3$ (00-006-0117) and $SmO(OH)$ (00-013-0168) were observed (*).

Figure SI 3: PXRD patterns of $RE_5Ti_2O_{11}(OH)$ series of compounds. (a) Calculated PXRD pattern of $Lu_5Ti_2O_{11}(OH)$ based on single crystal data. Observed PXRD patterns of hydrothermally grown (b) $Lu_5Ti_2O_{11}(OH)$, (c) $Yb_5Ti_2O_{11}(OH)$ and (d) $Tm_5Ti_2O_{11}(OH)$.

Figure SI 4: PXRD patterns of $\text{Ce}_2\text{Ti}_4\text{O}_{11}$. (a) Calculated powder pattern of $\text{Ce}_2\text{Ti}_4\text{O}_{11}$ based on single crystal structure refinement; (b) Observed PXRD pattern of the $\text{Ce}_2\text{Ti}_4\text{O}_{11}$ reaction. Impurities of $\text{Ce}(\text{OH})_3$ (00-054-1268) and Ti_2O_3 (01-071-0150) are highlighted using (*) and (\blacktriangle), respectively.

Figure SI 5: Single crystal Raman spectra of $\text{Ce}_2\text{Ti}_4\text{O}_{11}$, $\text{La}_5\text{Ti}_4\text{O}_{15}(\text{OH})$, $\text{Lu}_5\text{Ti}_2\text{O}_{11}(\text{OH})$ and $\text{Sm}_3\text{TiO}_5(\text{OH})_3$ compounds. The bands in the range of $3600\text{-}3500\text{ cm}^{-1}$ confirm the presence of hydroxide groups in $\text{La}_5\text{Ti}_4\text{O}_{15}(\text{OH})$, $\text{Lu}_5\text{Ti}_2\text{O}_{11}(\text{OH})$ and $\text{Sm}_3\text{TiO}_5(\text{OH})_3$ compounds, while $\text{Ce}_2\text{Ti}_4\text{O}_{11}$ did not exhibit the characteristic OH stretching vibration.

Figure SI 6: Polyhedral view of the two dimensional Ti–O–Ti lattice of $\text{La}_5\text{Ti}_4\text{O}_{15}(\text{OH})$, propagating infinitely in the *bc* plane.

Figure SI 7: Section of the crystal structure of $\text{La}_5\text{Ti}_4\text{O}_{11}(\text{OH})$ showing the connectivity between La–O–La lattice and Ti–O–Ti lattice along the *ac*-plane.

Figure SI 8: (a) Sm–O–Sm lattice of $\text{Sm}_3\text{TiO}_5(\text{OH})_3$ along *ab*-plane with propagation of the Sm–O–Sm lattice along the *a* and *b* axes; (b) partial structure of Sm–O–Sm chains in the $\text{Sm}_3\text{TiO}_5(\text{OH})_3$ structure showing the triangular units built from one $\text{Sm}(1)\text{O}_8$ and two $\text{Sm}(2)\text{O}_7$ units.

Figure SI 9: (a) The Sm–O–Ti–O–Sm lattice of $\text{Sm}_3\text{TiO}_5(\text{OH})_3$; (b) Connectivity between $\text{Sm}(1)\text{O}_8$ and $\text{Ti}(1)\text{O}_5$ units; (c) Connectivity between $\text{Sm}(2)\text{O}_7$ and $\text{Ti}(1)\text{O}_5$ units.

Synthesis

Synthesis of $\text{La}_5\text{Ti}_4\text{O}_{15}(\text{OH})$ and $\text{Er}_5\text{Ti}_4\text{O}_{15}(\text{OH})$

The $\text{La}_5\text{Ti}_4\text{O}_{15}(\text{OH})$ crystals were synthesized by a direct hydrothermal reaction of binary metal oxides. A total of 0.2 g of La_2O_3 (134.2 mg, 0.412 mmol) and TiO_2 (65.8 mg, 0.824 mmol) were used in a stoichiometric ratio of 1 : 2 with 0.4 mL of 20 M KOH. The crystals were colorless needles with an average length of 0.5 mm. In the case of the $\text{Er}_5\text{Ti}_4\text{O}_{15}(\text{OH})$, 0.2 g of Er_2O_3 (141.1 mg, 0.369 mmol) and TiO_2 (58.9 mg, 0.738 mmol) in a 1 : 2 molar ratio with 0.4 mL of 20 M KOH were used and pink crystals of $\text{Er}_5\text{Ti}_4\text{O}_{15}(\text{OH})$ were retrieved after washing with deionized water.

Synthesis of $\text{Lu}_5\text{Ti}_2\text{O}_{11}(\text{OH})$, $\text{Yb}_5\text{Ti}_2\text{O}_{11}(\text{OH})$ and $\text{Tm}_5\text{Ti}_2\text{O}_{11}(\text{OH})$

$\text{Lu}_5\text{Ti}_2\text{O}_{11}(\text{OH})$ was synthesized by using a mixture of Lu_2O_3 (142.7 mg, 0.359 mmol) and TiO_2 (57.3 mg, 0.717 mmol) in a 1 : 2 molar ratio with 0.4 mL of 20 M KOH. Similarly method was employed to synthesize $\text{Yb}_5\text{Ti}_2\text{O}_{11}\text{OH}$ and $\text{Tm}_5\text{Ti}_2\text{O}_{11}\text{OH}$ derivatives. For $\text{Yb}_5\text{Ti}_2\text{O}_{11}\text{OH}$ a mixture of Yb_2O_3 (142.3 mg, 0.361 mmol), and TiO_2 (57.7 mg, 0.722 mmol) and for $\text{Tm}_5\text{Ti}_2\text{O}_{11}\text{OH}$ a mixture of Tm_2O_3 (141.4 mg, 0.367 mmol) and TiO_2 (58.6 mg, 0.733 mmol) were used. The single crystals of $\text{Lu}_5\text{Ti}_2\text{O}_{11}(\text{OH})$ with the average size of ~0.5 mm on the edge.

Synthesis of $\text{Sm}_3\text{TiO}_5(\text{OH})$

The best reaction to synthesize single crystals of $\text{Sm}_3\text{TiO}_5(\text{OH})$ is 3 : 2 molar ratio between Sm_2O_3 and TiO_2 . Herein, a total of 0.2 g of Sm_2O_3 (13.5 mg, 0.498 mmol) and TiO_2 (26.5 mg, 0.332 mmol) were used with 0.4 mL of 20 M KOH. The resulted crystals were crystals were yellow blocks with an average size of 1 mm.

Synthesis of Ce₂Ti₄O₁₁

The single crystals of Ce₂Ti₄O₁₁ were synthesized by a direct hydrothermal reaction using binary metal oxides of Ce₂O₃ (101.4 mg, 0.309 mmol) and TiO₂ (98.6 mg, 1.235 mmol) in a 1 : 4 molar ratio, with a 0.4 mL of 6 M CsF. The resulting crystals were dark red polyhedra with an average size of 0.3 mm.

Synthesis of RE₂Ti₂O₇ (RE = La, Pr, Nd, Gd– Lu) Single Crystals

All the RE₂Ti₂O₇ phases were synthesized mainly using 30 M CsF as the mineralizer. However, in some cases 20 M KOH also produced RE₂Ti₂O₇ type compounds. Herein, two classes of RE₂Ti₂O₇ were mainly observed. First series of RE₂Ti₂O₇ (RE = La, Pr and Nd) crystalize in monoclinic crystal system with space group of *P2*₁ and second series is pyrochlore-RE₂Ti₂O₇ compounds crystalize in cubic *Fd-3m* space group. In all the cases, reaction stoichiometry was 1 : 2 between RE₂O₃ and TiO₂, except for Tb-oxide reaction. In Tb-oxide reaction, Tb₄O₇ was used in the ratio of 1 : 4 with TiO₂. All the reactions were performed using a total of 0.2 g of reactants with 0.4 mL of appropriate mineralizer. The detail amount of reactants for each reactions are summarized below.

For La₂Ti₂O₇: 134.2 mg (0.412 mmol) of La₂O₃ and 65.8 mg (0.824mmol) of TiO₂; for Pr₂Ti₂O₇: 134.7 mg (0.409 mmol) of Pr₂O₃ and 65.3 mg (0.817 mmol) of TiO₂; for Nd₂Ti₂O₇: 135.6 mg (0.403 mmol) of Nd₂O₃ and 64.4 mg (0.806 mmol) of TiO₂; for Gd₂Ti₂O₇: 138.8 mg of (0.383 mmol) Gd₂O₃ and 61.2 mg (0.766 mmol) of TiO₂; for Tb₂Ti₂O₇: 140.1 mg (0.187 mmol) of Tb₄O₇ and 59.9 mg (0.750 mmol) of TiO₂; for Dy₂Ti₂O₇: 140.0 mg (0.375 mmol) of Dy₂O₃ and 60.0 mg (0.751 mmol) of TiO₂; for Ho₂Ti₂O₇: 140.6 mg of (0.372 mmol) Ho₂O₃ and 59.4 mg of (0.744 mmol) TiO₂; for Er₂Ti₂O₇: 141.1 mg (0.369 mmol) of Er₂O₃ and 58.9 mg (0.738 mmol) of

TiO₂; for Tm₂Ti₂O₇: 141.4 mg (0.367 mmol) of Tm₂O₃ and 58.6 mg (0.733 mmol) of TiO₂; for Yb₂Ti₂O₇: 142.3 mg (0.361 mmol) of Yb₂O₃ and 57.7 mg (0.722 mmol) of TiO₂; for Lu₂Ti₂O₇: 142.7 mg (0.359 mmol) of Lu₂O₃ and 57.3 mg (0.717 mmol) of TiO₂.

Structure Refinement of Lu₅Ti₂O₁₁(OH)

Data collection and processing proceeded in the same manner as all the compounds in this study as described in the main body of the manuscript. The primary atomic positions for the Lu, Ti and O atoms were easily identified using intrinsic phasing and subsequent refinement from the difference electron density map. The Lu and Ti sites were easily distinguishable on the basis of their bond lengths, as well as their anisotropic displacement parameters. However, significant electron density remained in the difference electron density map, suggesting some unaccounted for twinning or disorder may be present. Both circumstances are present in the literature surrounding this structure type. After application of the twin law [-1 0 -1 0 -1 0 0 1] (with refined BASF of 0.127) there was still a significant peak of electron density remaining within the lutetium oxide framework, and having appropriate interatomic distances to oxygen to suggest a disordered arrangement of lutetium. Free refinement of the occupancy of this disordered site (Lu4) suggested it was approximately 3.4% occupied by Lu. Occupancy values for the remaining Lu sites were appropriately reduced to maintain a stoichiometry of “Lu₅Ti₂O₁₂”. Further, the shape of the anisotropic displacement parameter of the Lu3 site suggested it should be split into two disordered positions. These steps produced reasonable ADPs for all Lu atoms and accounted for all of the significant remaining electron density (the highest remaining peak is found to be 1.28 e/Å³).

Raman spectroscopy revealed the presence of OH in the structure, and the O2 site was found to be underbonded by a bond valence sum analysis. A partially-occupied H atom was assigned to a sterically-favorable position about the O2 atom. Importantly, this resulted in the charge balanced formula of $\text{Lu}_5\text{Ti}_2\text{O}_{11}(\text{OH})$. Other possibilities for charge balance were considered, including those that may make use of the disordered site identified as Lu4. However, the colorless nature of the crystals, the presence of the OH stretching vibration in the Raman spectrum, the elemental analysis by EDX, and the local geometries of the crystallographic sites were all supportive of $\text{Lu}_5\text{Ti}_2\text{O}_{11}(\text{OH})$. The final R1 and wR2 values for this model were 0.0294 and 0.0701, respectively. The powder X-ray diffraction pattern calculated from the single crystal structural model is in excellent agreement with the experimental PXRD data (Figure SI 3).

Table SI 1: Crystallographic data for hydrothermally grown Er₅Ti₄O₁₅(OH).

empirical formula	Er ₅ Ti ₄ O ₁₅ (OH)
formula weight (g/mol)	1284.91
crystal system	orthorhombic
space group, Z	<i>Pnmm</i> (no. 58), 4
temperature, K	298(2)
crystal size (mm)	0.12 x 0.08 x 0.02
<i>a</i> , Å	29.7954(13)
<i>b</i> , Å	5.3286(2)
<i>c</i> , Å	7.4498(3)
volume, Å ³	1182.79(8)
calculated density (µg/m ³)	7.216
absorption coefficient (mm ⁻¹)	37.694
F(000)	2228
Tmax, Tmin	1.0000, 0.4169
Θ range for data	2.734-33.355
reflections collected	2349
data/restraints/parameters	2349/0/132
final R [<i>I</i> > 2σ(<i>I</i>)] R1, wR2	0.0244/0.0553
final R (all data) R1, wR2	0.0297/0.0566
goodness-of-fit on F ²	1.140
largest diff. peak/hole, e/ Å ³	2.241/-2.155

Table SI 2: Selected bond lengths (Å) of $\text{La}_5\text{Ti}_4\text{O}_{15}(\text{OH})$ and $\text{Er}_5\text{Ti}_4\text{O}_{15}(\text{OH})$.

$\text{La}_5\text{Ti}_4\text{O}_{15}(\text{OH})$		$\text{Er}_5\text{Ti}_4\text{O}_{15}(\text{OH})$	
La(1)O₈		Er(1)O₈	
La(1)–O(1) x 2	2.631(3)	Er(1)–O(1) x 2	2.418(4)
La(1)–O(4) x 2	2.567(3)	Er(1)–O(4) x 2	2.470(4)
La(1)–O(5) x 2	2.500(3)	Er(1)–O(5) x 2	2.353(4)
La(1)–O(6)	2.517(3)	Er(1)–O(6)	2.296(5)
La(1)–O(7)	2.586(4)	Er(1)–O(7)	2.342(5)
La(2)O₇		Er(2)O₇	
La(2)–O(2) x 2	2.360(4)	Er(2)–O(2) x 2	2.185(5)
La(2)–O(3)	2.567(4)	Er(2)–O(3)	2.308(5)
La(2)–O(4) x 2	2.471(3)	Er(2)–O(4) x 2	2.297(4)
La(2)–O(5) x 2	2.503(3)	Er(2)–O(5) x 2	2.443(4)
La(3)O₈		Er(3)O₈	
La(3)–O(2) x 2	2.366(3)	Er(3)–O(2) x 2	2.234(3)
La(3)–O(4) x 2	2.603(3)	Er(3)–O(4) x 2	2.494(4)
La(3)–O(5) x 2	2.605(3)	Er(3)–O(5) x 2	2.463(4)
La(3)–O(6) x 2	2.531(3)	Er(3)–O(6) x 2	2.380(3)
La(4)O₈		Er(4)O₈	
La(4)–O(1) x 2	2.652(3)	Er(4)–O(1) x 2	2.444(4)
La(4)–O(7)	2.528(4)	Er(4)–O(7)	2.301(5)
La(4)–O(8) x 2	2.567(3)	Er(4)–O(8) x 2	2.433(4)
La(4)–O(10) x 2	2.504(3)	Er(4)–O(10) x 2	2.293(4)
La(4)–O(11)	2.457(4)	Er(4)–O(11)	2.234(5)
La(5)O₈		Er(5)O₈	
La(5)–O(8) x 2	2.404(3)	Er(5)–O(8) x 2	2.244(4)
La(5)–O(9)	2.533(4)	Er(5)–O(9)	2.291(5)
La(5)–O(10) x 2	2.711(3)	Er(5)–O(10) x 2	2.242(4)
La(5)–O(10) x 2	2.758(3)	Er(5)–O(10) x 2	2.643(4)
La(5)–O(11)	2.512(4)	Er(5)–O(11)	2.253(5)
Ti(1)O₆		Ti(1)O₆	
Ti(1)–O(1)	2.267(3)	Ti(1)–O(1)	2.235(4)
Ti(1)–O(3)	1.979(3)	Ti(1)–O(3)	1.908(4)
Ti(1)–O(4)	1.803(3)	Ti(1)–O(4)	1.801(4)
Ti(1)–O(5)	1.866(3)	Ti(1)–O(5)	1.858(4)
Ti(1)–O(7)	2.107(3)	Ti(1)–O(7)	2.014(4)
Ti(1)–O(8)	2.027(3)	Ti(1)–O(8)	2.043(4)
Ti(2)O₆		Ti(2)O₆	
Ti(2)–O(1)	1.827(3)	Ti(2)–O(1)	1.823(4)
Ti(2)–O(8)	1.920(3)	Ti(2)–O(8)	1.920(4)
Ti(2)–O(9)	1.968(3)	Ti(2)–O(9)	1.911(4)
Ti(2)–O(10)	1.978(3)	Ti(2)–O(10)	1.997(4)
Ti(2)–O(10)	2.184(3)	Ti(2)–O(10)	2.234(3)
Ti(2)–O(11)	1.998(3)	Ti(2)–O(11)	1.997(4)

Table SI 3: Selected bond lengths (Å) of $\text{Sm}_3\text{TiO}_5(\text{OH})_3$, $\text{Lu}_5\text{Ti}_2\text{O}_{11}(\text{OH})$, and $\text{Ce}_2\text{Ti}_4\text{O}_{11}$.

$\text{Sm}_3\text{TiO}_5(\text{OH})_3$		$\text{Lu}_5\text{Ti}_2\text{O}_{11}(\text{OH})$		$\text{Ce}_2\text{Ti}_4\text{O}_{11}$	
Sm(1)O₈		Lu(1)O₇		Ce(1)O₈	
Sm(1)–O(1) x 2	2.404(3)	Lu(1)–O(1) x 2	2.224(9)	Ce(1)–O(1)	2.382(4)
))))))
Sm(1)–O(2) x 2	2.432(3)	Lu(1)–O(1) x 2	2.324(9)	Ce(1)–O(2)	2.408(4)
))))))
Sm(1)–O(3) x 2	2.555(3)	Lu(1)–O(2) x 2	2.335(10)	Ce(1)–O(3)	2.412(4)
))))))
Sm(1)–O(4)	2.432(5)	Lu(1)–O(4)	2.292(12)	Ce(1)–O(3)	2.439(4)
))))))
Sm(1)–O(5)	2.445(4)	Lu(2)O₇		Ce(1)–O(4)	2.450(4)
))))
Sm(2)O₇		Lu(2)–O(1) x 2	2.257(9)	Ce(1)–O(5)	2.675(4)
Sm(2)–O(1)	2.375(3)	Lu(2)–O(2) x 2	2.282(10)))
))))	Ce(1)–O(1)	2.725(4)
Sm(2)–O(1)	2.444(3)	Lu(2)–O(2) x 2	2.331(10)))
))))	Ti(1)O₆	
Sm(2)–O(2)	2.296(3)	Lu(2)–O(4)	2.338(12)	Ti(1)–O(1)	1.961(4)
))))))
Sm(2)–O(2)	2.359(3)	Lu(3A)O₆		Ti(1)–O(2)	2.039(4)
))))
Sm(2)–O(3)	2.337(3)	Lu(3A)–O(2) x 2	2.14(6)	Ti(1)–O(4)	1.879(4)
))))))
Sm(2)–O(3)	2.491(3)	Lu(3A)–O(2) x 2	2.41(7)	Ti(1)–O(4)	1.932(4)
))))))
Sm(2)–O(5)	2.529(2)	Lu(3A)–O(3) x 2	2.238(15)	Ti(1)–O(5)	1.928(4)
))))))
Ti(1)O₅		Lu(3B)O₆		Ti(1)–O(6)	2.139(3)
Ti(1)–O(1) x 2	1.944(3)	Lu(3A)–O(2) x 2	2.15(6)	Ti(2)O₆	
))))		
Ti(1)–O(2) x 2	1.925(3)	Lu(3A)–O(2) x 2	2.40(7)	Ti(2)–O(1)	1.918(4)
))))))
Ti(1)–O(4)	1.764(4)	Lu(3A)–O(3) x 2	2.236(14)	Ti(2)–O(2)	1.750(4)
))))))
		Lu(4)O₆		Ti(2)–O(3)	2.021(4)
		Lu(4)–O(2) x 4	2.239(10)	Ti(2)–O(5)	2.385(4)
		Lu(4)–O(2) x 2	2.143(11)	Ti(2)–O(5)	2.068(4)
		Ti(1)O₆		Ti(2)–O(6)	
		Ti(1)–O(1) x 2	1.922(8)		
		Ti(1)–O(3) x 2	1.904(8)		
		Ti(1)–O(4) x 2	2.047(8)		

Table SI 4: Bond valence sum calculations of $\text{La}_5\text{Ti}_4\text{O}_{15}(\text{OH})$ and $\text{Er}_5\text{Ti}_4\text{O}_{15}(\text{OH})$.

$\text{La}_5\text{Ti}_4\text{O}_{15}(\text{OH})$		$\text{Er}_5\text{Ti}_4\text{O}_{15}(\text{OH})$	
La(1)O_8		Er(1)O_8	
La(1)–O(1) x 2	0.578	Er(1)–O(1) x 2	0.616
La(1)–O(4) x 2	0.688	Er(1)–O(4) x 2	0.544
La(1)–O(5) x 2	0.824	Er(1)–O(5) x 2	0.746
La(1)–O(6)	0.394	Er(1)–O(6)	0.435
La(1)–O(7)	0.327	Er(1)–O(7)	0.384
$\Sigma\text{La(1)}$	2.811	$\Sigma\text{Er(1)}$	2.734
La(2)O_7		Er(2)O_7	
La(2)–O(2) x 2	1.204	Er(2)–O(2) x 2	1.174
La(2)–O(3)	0.344	Er(2)–O(3)	0.421
La(2)–O(4) x 2	0.892	Er(2)–O(4) x 2	0.864
La(2)–O(5) x 2	0.818	Er(2)–O(5) x 2	0.586
$\Sigma\text{La(2)}$	3.256	$\Sigma\text{Er(2)}$	3.048
La(3)O_8		Er(3)O_8	
La(3)–O(2) x 2	1.184	Er(3)–O(2) x 2	1.028
La(3)–O(4) x 2	0.624	Er(3)–O(4) x 2	0.510
La(3)–O(5) x 2	0.620	Er(3)–O(5) x 2	0.544
La(3)–O(6) x 2	0.758	Er(3)–O(6) x 2	0.694
$\Sigma\text{La(3)}$	3.186	$\Sigma\text{Er(3)}$	2.785
La(4)O_8		Er(4)O_8	
La(4)–O(1) x 2	0.546	Er(4)–O(1) x 2	0.584
La(4)–O(7)	0.382	Er(4)–O(7)	0.429
La(4)–O(8) x 2	0.688	Er(4)–O(8) x 2	0.600
La(4)–O(10) x 2	0.816	Er(4)–O(10) x 2	0.878
La(4)–O(11)	0.463	Er(4)–O(11)	0.514
$\Sigma\text{La(4)}$	2.865	$\Sigma\text{Er(4)}$	3.004
La(5)O_8		Er(5)O_8	
La(5)–O(8) x 2	1.068	Er(5)–O(8) x 2	1.002
La(5)–O(9)	0.377	Er(5)–O(9)	0.441
La(5)–O(10) x 2	0.466	Er(5)–O(10) x 2	1.006
La(5)–O(10) x 2	0.410	Er(5)–O(10) x 2	0.340

La(5)–O(11)	0.399	Er(5)–O(11)	0.489
ΣLa(5)	2.959	ΣEr(5)	3.278
	Ti(1)O₆		Ti(1)O₆
Ti(1)–O(1)	0.295	Ti(1)–O(1)	0.321
Ti(1)–O(3)	0.641	Ti(1)–O(3)	0.778
Ti(1)–O(4)	1.033	Ti(1)–O(4)	1.039
Ti(1)–O(5)	0.871	Ti(1)–O(5)	0.890
Ti(1)–O(7)	0.454	Ti(1)–O(7)	0.584
Ti(1)–O(8)	0.564	Ti(1)–O(8)	0.540
ΣTi(1)	3.858	ΣTi(1)	4.151
	Ti(2)O₆		Ti(2)O₆
Ti(2)–O(1)	0.968	Ti(2)–O(1)	0.979
Ti(2)–O(8)	0.753	Ti(2)–O(8)	0.753
Ti(2)–O(9)	0.661	Ti(2)–O(9)	0.770
Ti(2)–O(10)	0.644	Ti(2)–O(10)	0.611
Ti(2)–O(10)	0.369	Ti(2)–O(10)	0.322
Ti(2)–O(11)	0.610	Ti(2)–O(11)	0.611
ΣTi(2)	4.005	ΣTi(2)	4.045

Table SI 5: Bond valence sum calculations of $\text{Sm}_3\text{TiO}_5(\text{OH})_3$, $\text{Lu}_5\text{Ti}_2\text{O}_{11}(\text{OH})$ and $\text{Ce}_2\text{Ti}_4\text{O}_{11}$.

Sm₃TiO₅(OH)₃		Lu₅Ti₂O₁₁(OH)		Ce₂Ti₄O₁₁	
Sm(1)O₈		Lu(1)O₇		Ce(1)O₇	
Sm(1)–O(1) x	0.85	Lu(1)–O(1) x 2	1.002	Ce(1)–O(1)	0.536
2	4				
Sm(1)–O(2) x	0.79	Lu(1)–O(1) x 2	0.766	Ce(1)–O(2)	0.499
2	2				
Sm(1)–O(3) x	0.56	Lu(1)–O(2) x 2	0.748	Ce(1)–O(3)	0.494
2	2				
Sm(1)–O(4)	0.39	Lu(1)–O(4)	0.423	Ce(1)–O(3)	0.459
	6				
Sm(1)–O(5)	0.37	ΣLu(1)	2.939	Ce(1)–O(4)	0.446
	9				
ΣSm(1)	2.98	Lu(2)O₇		Ce(1)–O(5)	0.243
	1				
	Sm(2)O₇	Lu(2)–O(1) x 2	0.920	Ce(1)–O(1)	0.212
Sm(2)–O(1)	0.46	Lu(2)–O(2) x 2	0.872	ΣCe(1)	2.888
	0				
Sm(2)–O(1)	0.38	Lu(2)–O(2) x 2	0.752	Ti(1)O₆	
	2				
Sm(2)–O(2)	0.57	Lu(2)–O(4)	0.366	Ti(1)–O(1)	0.674
	0				
Sm(2)–O(2)	0.48	ΣLu(2)	2.911	Ti(1)–O(2)	0.546
	2				
Sm(2)–O(3)	0.50	Lu(3)O₆		Ti(1)–O(4)	0.841
	7				
Sm(2)–O(3)	0.33	Lu(3)–O(2) x 2	1.242	Ti(1)–O(4)	0.729

Sm(2)–O(5)	0.30	6 Lu(3)–O(2) x 2	0.632	Ti(1)–O(5)	0.737
ΣSm(2)	3.04	2 Lu(3)–O(3) x 2	0.982	Ti(1)–O(6)	0.417
	0				
		Ti(1)O₅	ΣLu(3)	2.856	ΣTi(1)
Ti(1)–O(1) x	1.40	Lu(4)O₆		Ti(2)O₆	3.943
2	8				
Ti(1)–O(2) x	1.48	Lu(4)–O(2) x 4	1.948	Ti(2)–O(1)	
2	2				0.757
Ti(1)–O(4)	1.14	Lu(4)–O(2) x 2	1.230	Ti(2)–O(2)	0.881
	8				
ΣTi(1)	4.03	ΣLu(4)	3.179	Ti(2)–O(3)	1.192
	7				
		Ti(1)O₆		Ti(2)–O(5)	0.573
		Ti(1)–O(1) x 2	1.518	Ti(2)–O(5)	0.214
		Ti(1)–O(3) x 2	1.556	Ti(2)–O(6)	0.505
		Ti(1)–O(4) x 2	1.086	ΣTi(2)	4.122
		ΣTi(1)	4.159		

Table SI 6: EDX of reported rare-earth titanates with experimental and expected RE:Ti ratios.

Structure	RE/Ti EDX ratio (%)	Experimental ratio	Expected ratio
La₅Ti₄O₁₅(OH)	22.1/23.5	0.94:1	1.25:1
Er₅Ti₄O₁₅(OH)	18.6/16.5	1.13:1	1.25:1

Ce₂Ti₄O₁₁	9.8/20.7	0.47:1	0.5:1
Sm₃TiO₅(OH)₃	34.3/11.7	2.93:1	3.0:1
Tm₅Ti₂O₁₁(OH)	22.8/9.7	2.35:1	2.5:1
Yb₅Ti₂O₁₁(OH)	27/12	2.25:1	2.5:1
Lu₅Ti₂O₁₁(OH)	29.7/10.8	2.75:1	2.5:1

Table SI 7: Summary of M - M bond distances for $RE_5M_2O_{12}$ ($M = \text{Ru, Re, Mo}$) and $RE_5Ti_2O_{11}(\text{OH})$ compounds.

Structure	M–M bond distance (short) (Å)	M–M bond distance (long) (Å)	Reference
Pr ₅ Ru ₂ O ₁₂	2.8038	3.1450	53
Eu ₅ Ru ₂ O ₁₂	2.780	3.091	53
Gd ₅ Ru ₂ O ₁₂	2.774	3.084	53
Tb ₅ Ru ₂ O ₁₂	2.7765	3.0649	53
Eu ₅ Mo ₂ O ₁₂	2.523	3.265	69
Tb ₅ Mo ₂ O ₁₂	2.510	3.243	69
Dy ₅ Mo ₂ O ₁₂	2.505	3.233	69
Ho ₅ Mo ₂ O ₁₂	2.499	3.219	69
Y ₅ Mo ₂ O ₁₂	2.496	3.221	68
Er ₅ Mo ₂ O ₁₂	2.494	3.219	69
Y ₅ Re ₂ O ₁₂	2.4466	3.2138	54
Tm ₅ Re ₂ O ₁₂	2.455	3.219	55
Ho ₅ Re ₂ O ₁₂	2.436	3.201	56
Lu ₅ Ti ₂ O ₁₁ (OH)	2.799(8)	3.026(8)	this work

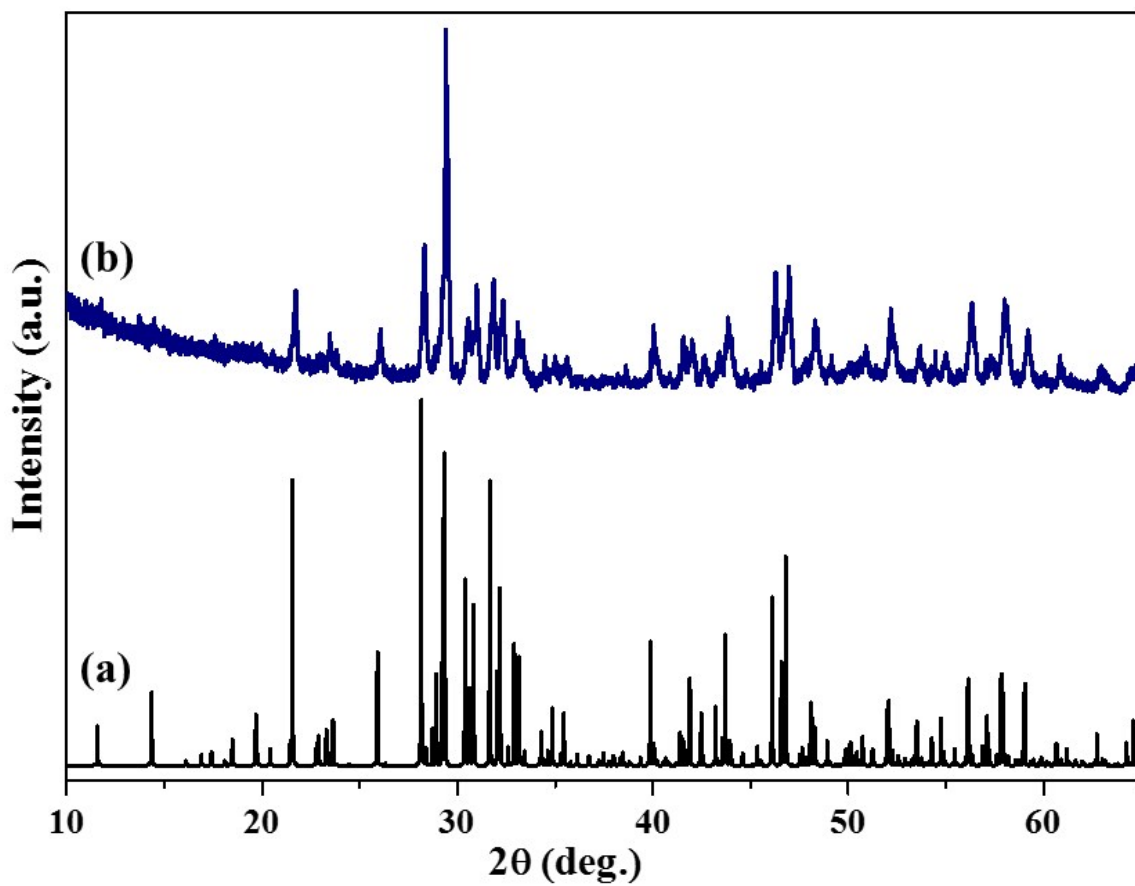


Figure SI 1: PXRd patterns of $\text{La}_5\text{Ti}_4\text{O}_{15}(\text{OH})$. (a) Simulated powder pattern based on single crystal data of $\text{La}_5\text{Ti}_4\text{O}_{15}(\text{OH})$; (b) Observed PXRd of $\text{La}_5\text{Ti}_4\text{O}_{15}(\text{OH})$.

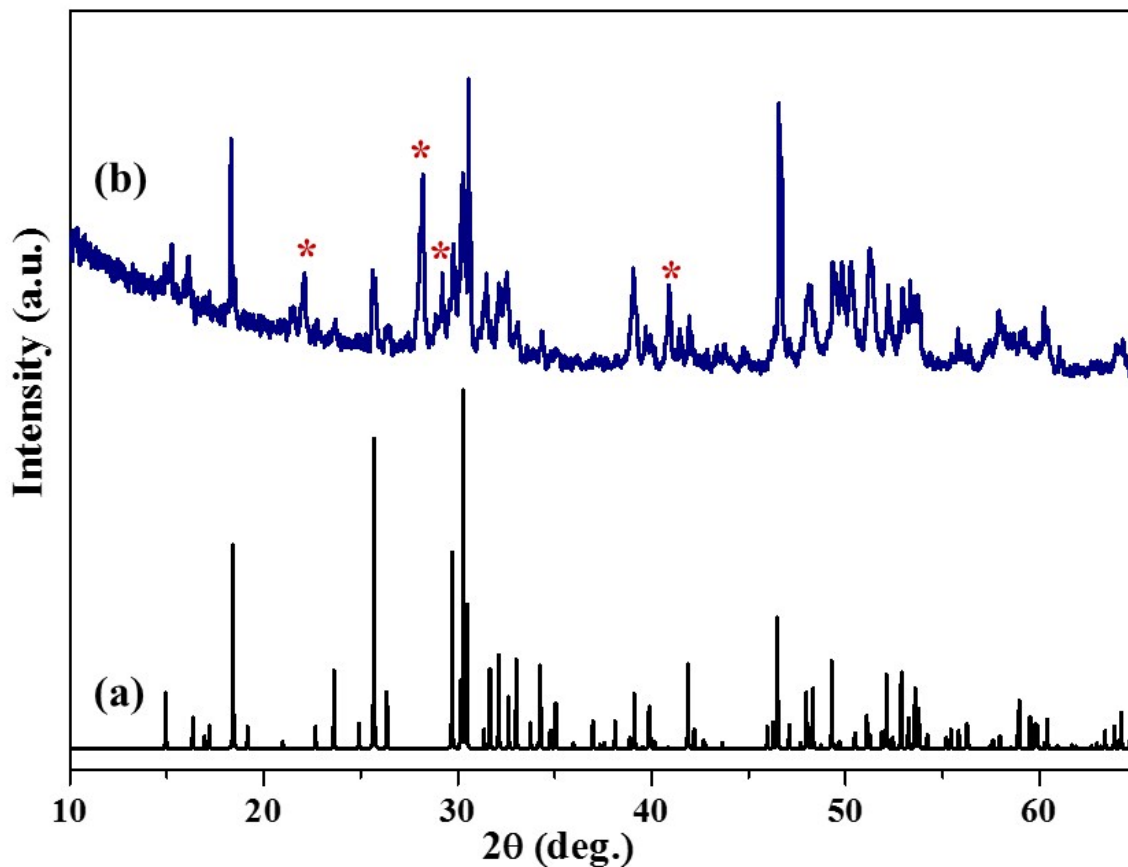


Figure SI 2: PXRD patterns of $\text{Sm}_3\text{TiO}_5(\text{OH})_3$. (a) Simulated powder pattern based on single crystal structure data of $\text{Sm}_3\text{TiO}_5(\text{OH})_3$; (b) Observed PXRD pattern for the $\text{Sm}_3\text{TiO}_5(\text{OH})_3$ reaction and impurities of $\text{Sm}(\text{OH})_3$ (00-006-0117) and $\text{SmO}(\text{OH})$ (00-013-0168) were observed (*).

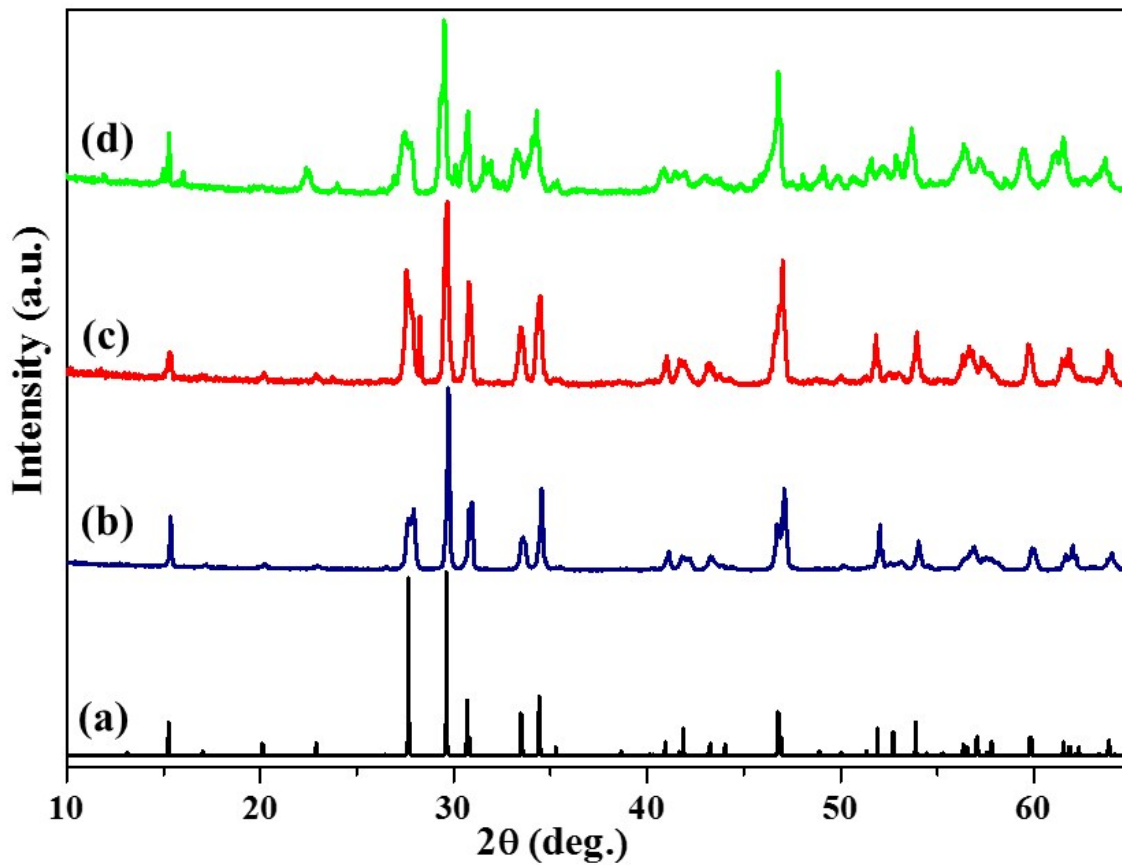


Figure SI 3: PXR D patterns of $RE_5Ti_2O_{11}(OH)$ series of compounds. (a) Calculated PXR D pattern of $Lu_5Ti_2O_{11}(OH)$ based on single crystal data. Observed PXR D patterns of hydrothermally grown (b) $Lu_5Ti_2O_{11}(OH)$, (c) $Yb_5Ti_2O_{11}(OH)$ and (d) $Tm_5Ti_2O_{11}(OH)$.

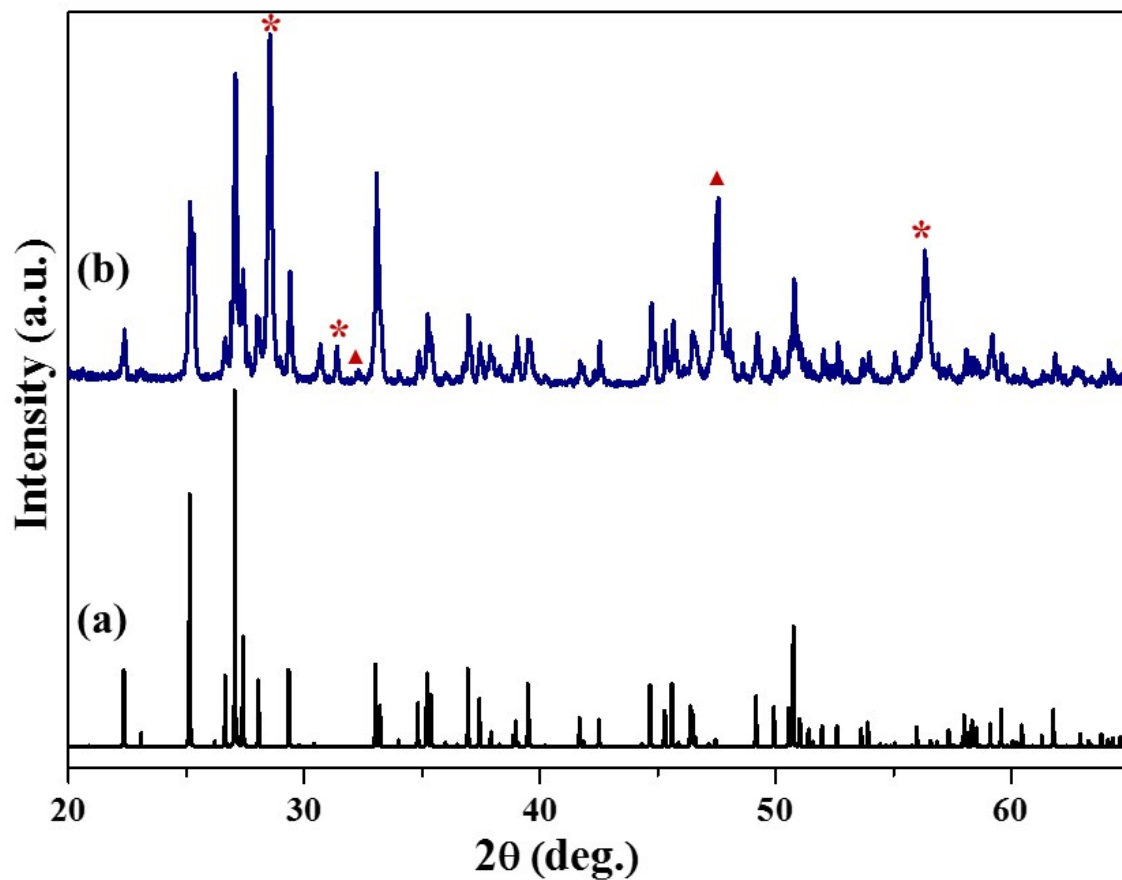


Figure SI 4: PXR D patterns of $\text{Ce}_2\text{Ti}_4\text{O}_{11}$. (a) Calculated powder pattern of $\text{Ce}_2\text{Ti}_4\text{O}_{11}$ based on single crystal structure refinement; (b) Observed PXR D pattern of the $\text{Ce}_2\text{Ti}_4\text{O}_{11}$ reaction. Impurities of $\text{Ce}(\text{OH})_3$ (00-054-1268) and Ti_2O_3 (01-071-0150) are highlighted using (*) and (▲), respectively.

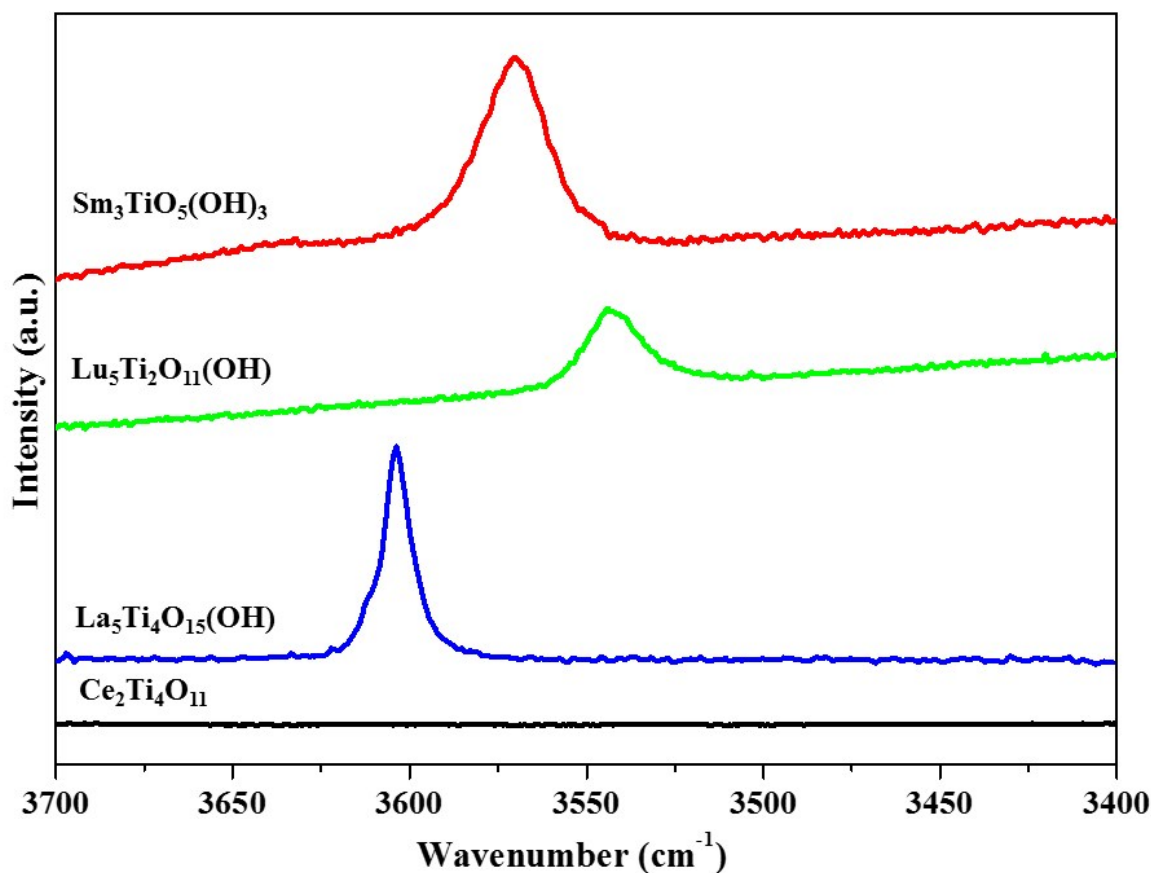


Figure SI 5: Single crystal Raman spectra of $\text{Ce}_2\text{Ti}_4\text{O}_{11}$, $\text{La}_5\text{Ti}_4\text{O}_{15}(\text{OH})$, $\text{Lu}_5\text{Ti}_2\text{O}_{11}(\text{OH})$ and $\text{Sm}_3\text{TiO}_5(\text{OH})_3$ compounds. The bands in the range of $3600\text{-}3500\text{ cm}^{-1}$ confirm the presence of hydroxide groups in $\text{La}_5\text{Ti}_4\text{O}_{15}(\text{OH})$, $\text{Lu}_5\text{Ti}_2\text{O}_{11}(\text{OH})$ and $\text{Sm}_3\text{TiO}_5(\text{OH})_3$ compounds, while $\text{Ce}_2\text{Ti}_4\text{O}_{11}$ did not exhibit the characteristic OH stretching vibration. In these structures, the hydrogen atom location is significantly influenced by the sterics of the framework, and lattice stability from hydrogen bonding becomes a rather minor contribution. Thus, in these structures, we observe very weak hydrogen bonding, with vibrations within the region expected for a free OH^- group ($3530\text{-}3622\text{ cm}^{-1}$, based on the analysis of various minerals in E. Libowitzky, *Monatsch. Chem.* 1999, **130**, 1047-1059). Correspondingly, any O-H---O angles in these structures are generally bent (113.4° to 153.9°), also supporting the concept that the hydrogen atoms participate in minimal attractive hydrogen bonding.

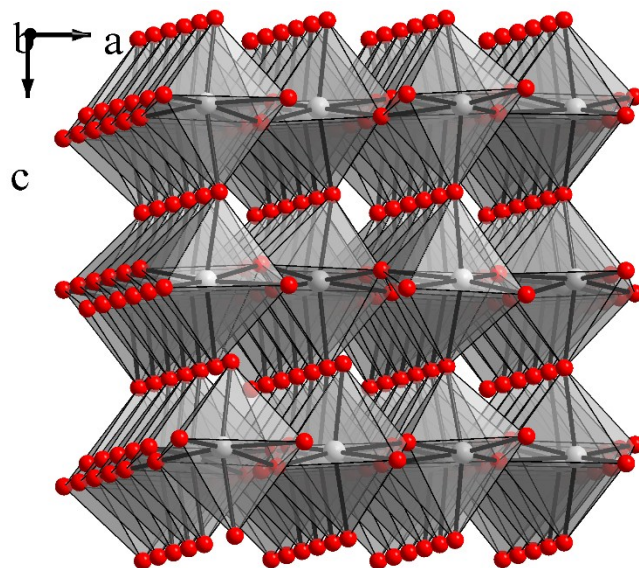


Figure SI 6: Polyhedral view of the two dimensional Ti–O–Ti lattice of $\text{La}_5\text{Ti}_4\text{O}_{15}(\text{OH})$, propagating infinitely in the bc plane.

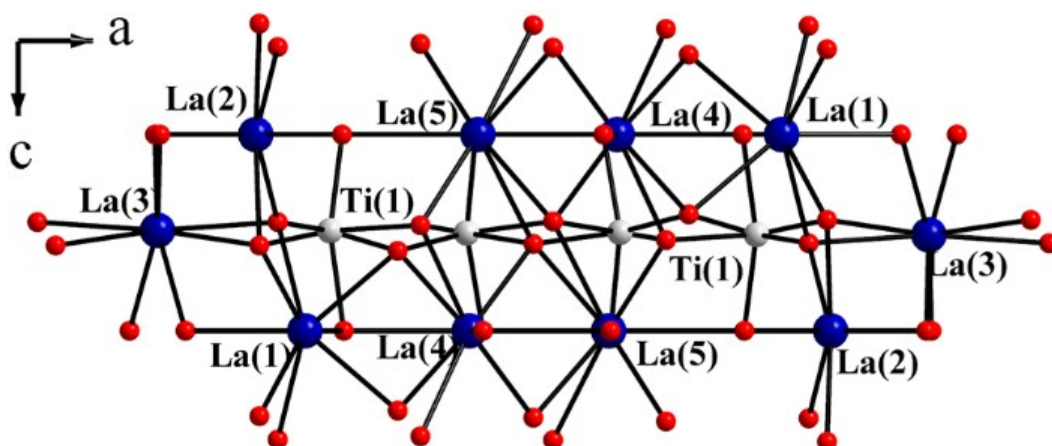


Figure SI 7: Section of the crystal structure of $\text{La}_5\text{Ti}_4\text{O}_{11}(\text{OH})$ showing the connectivity between La–O–La lattice and Ti–O–Ti lattice along the ac -plane.

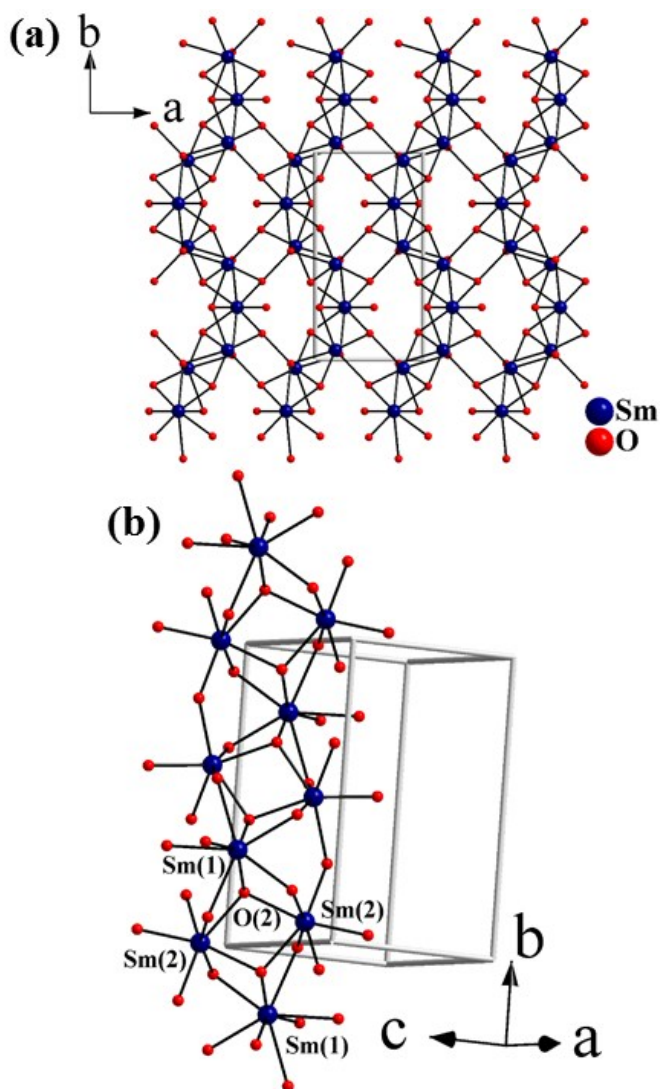


Figure SI 8: (a) Sm–O–Sm lattice of $\text{Sm}_3\text{TiO}_5(\text{OH})_3$ along ab -plane with propagation of the Sm–O–Sm lattice along the a and b axes; (b) partial structure of Sm–O–Sm chains in the $\text{Sm}_3\text{TiO}_5(\text{OH})_3$ structure showing the triangular units built from one Sm(1) O_8 and two Sm(2) O_7 units.

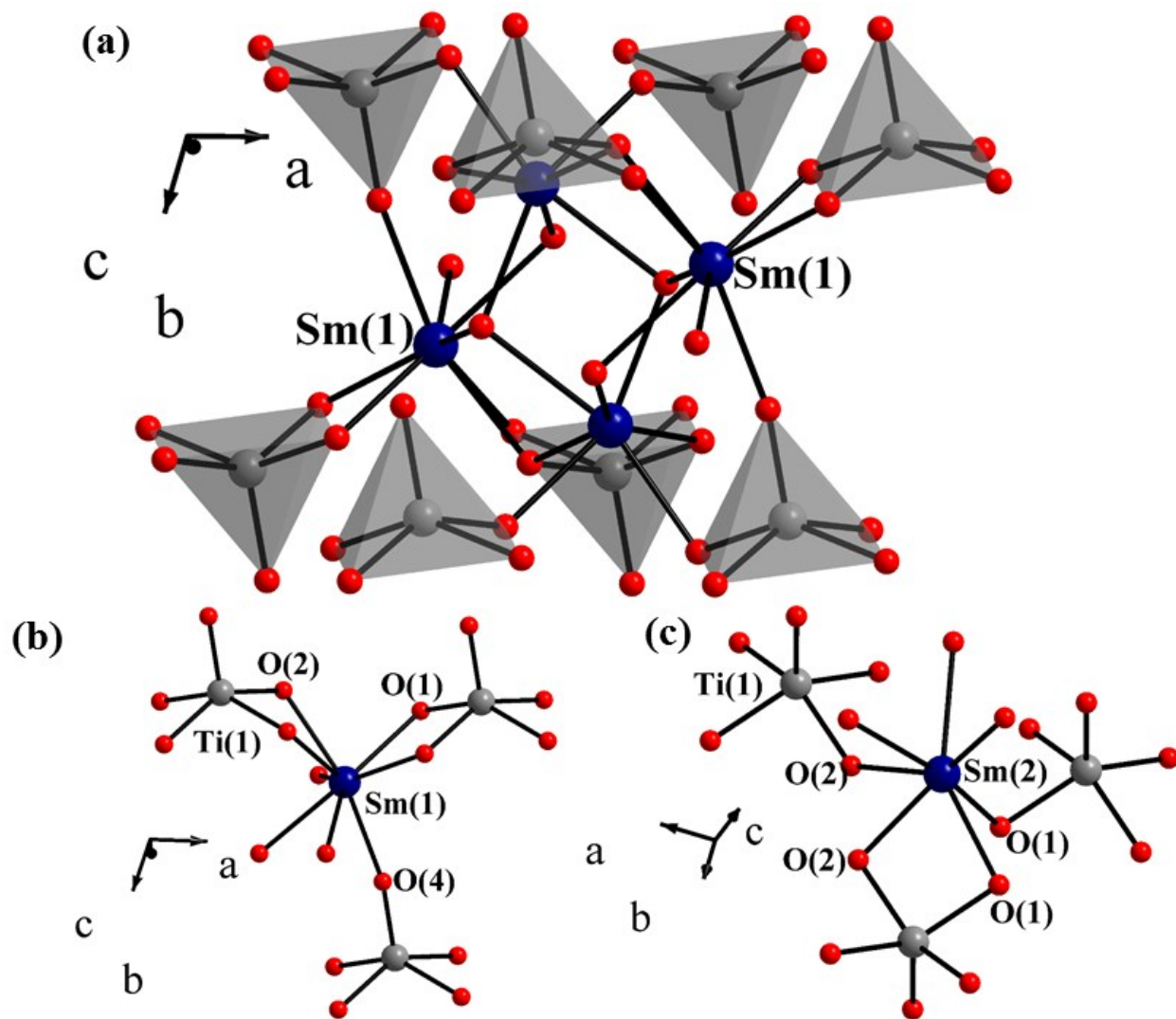


Figure SI 9: (a) The Sm–O–Ti–O–Sm lattice of $\text{Sm}_3\text{TiO}_5(\text{OH})_3$; (b) Connectivity between $\text{Sm}(1)\text{O}_8$ and $\text{Ti}(1)\text{O}_5$ units; (c) Connectivity between $\text{Sm}(2)\text{O}_7$ and $\text{Ti}(1)\text{O}_5$ units.